

Negative self-feedback induced enhancement and transition of spiking activity for class-3 excitability

Li Li(黎丽), Zhiguo Zhao(赵志国), and Huaguang Gu(古华光)
Citation: Chin. Phys. B, 2022, 31 (**7**): 070506. DOI: 10.1088/1674-1056/ac4a63
Journal homepage: http://cpb.iphy.ac.cn; http://iopscience.iop.org/cpb

What follows is a list of articles you may be interested in

Design and FPGA implementation of a memristor-based multi-scroll hyperchaotic system

Sheng-Hao Jia(贾生浩), Yu-Xia Li(李玉霞), Qing-Yu Shi(石擎宇), and Xia Huang(黄霞)
Chin. Phys. B, 2022, 31 (**7**): 070505. DOI: 10.1088/1674-1056/ac4a71

The transition from conservative to dissipative flows in class-B laser model with fold-Hopf bifurcation and coexisting attractors

Yue Li(李月), Zengqiang Chen(陈增强), Mingfeng Yuan(袁明峰), and Shijian Cang(仓诗建)
Chin. Phys. B, 2022, 31 (**6**): 060503. DOI: 10.1088/1674-1056/ac43a2

The dynamics of a memristor-based Rulkov neuron with fractional-order difference

Yan-Mei Lu(卢艳梅), Chun-Hua Wang(王春华), Quan-Li Deng(邓全利), and Cong Xu(徐聪)
Chin. Phys. B, 2022, 31 (**6**): 060502. DOI: 10.1088/1674-1056/ac539a

Inferring interactions of time-delayed dynamic networks by random state variable resetting

Changbao Deng(邓长宝), Weinuo Jiang(蒋未诺), and Shihong Wang(王世红)
Chin. Phys. B, 2022, 31 (**3**): 030502. DOI: 10.1088/1674-1056/ac1e12

Dynamical response of a neuron-astrocyte coupling system under electromagnetic induction and external stimulation

Zhi-Xuan Yuan(袁治轩), Pei-Hua Feng(冯沛华), Meng-Meng Du(独盟盟), Ying Wu(吴莹)
Chin. Phys. B, 2020, 29 (**3**): 030504. DOI: 10.1088/1674-1056/ab7441

Negative self-feedback induced enhancement and transition of spiking activity for class-3 excitability

Li Li(黎丽)[1], Zhiguo Zhao(赵志国)[2,†], and Huaguang Gu(古华光)[3]

[1] *Guangdong Key Laboratory of Modern Control Technology, Institute of Intelligent Manufacturing, Guangdong Academy of Sciences, Guangzhou* 510070, *China*

[2] *School of Science, Henan Institute of Technology, Xinxiang* 453003, *China*

[3] *School of Aerospace Engineering and Applied Mechanics, Tongji University, Shanghai* 200092, *China*

(Received 26 October 2021; revised manuscript received 1 January 2022; accepted manuscript online 12 January 2022)

Post-inhibitory rebound (PIR) spike, which has been widely observed in diverse nervous systems with different physiological functions and simulated in theoretical models with class-2 excitability, presents a counterintuitive nonlinear phenomenon in that the inhibitory effect can facilitate neural firing behavior. In this study, a PIR spike induced by inhibitory stimulation from the resting state corresponding to class-3 excitability that is not related to bifurcation is simulated in the Morris–Lecar neuron. Additionally, the inhibitory self-feedback mediated by an autapse with time delay can evoke tonic/repetitive spiking from phasic/transient spiking. The dynamical mechanism for the PIR spike and the tonic/repetitive spiking is acquired with the phase plane analysis and the shape of the quasi-separatrix curve. The result extends the counterintuitive phenomenon induced by inhibition to class-3 excitability, which presents a potential function of inhibitory autapse and class-3 neuron in many neuronal systems such as the auditory system.

Keywords: post-inhibitory rebound spike, class 3 excitability, inhibitory autapse, neuronal firing

PACS: 05.45.–a, 87.19.lg **DOI:** 10.1088/1674-1056/ac4a63

1. Introduction

Neurons transmit information by generating action potentials or spikes.[1,2] According to different features of neuronal spike responses to constant depolarization current, Hodgkin identified three classes of excitability.[3,4] For neurons with class-1 excitability, repetitive (tonic) spiking with arbitrarily low firing frequency can be evoked. For neurons with class-2 excitability, repetitive (tonic) spiking is evoked with a nonzero critical frequency.[3,5,6] In contrast to repetitive (tonic) spiking of neurons with class-1 or class-2 excitabilities, transient (phasic) spiking is elicited for neurons with class-3 excitability; that is, only a few spikes are generated at the onset of the sustained depolarization current.[7] The distinct spiking patterns enable the neurons to have different coding properties. For example, in a noisy environment, phasic spiking neurons show a larger variability of the spike amplitude compared to tonic spiking neurons.[5] Phasic spiking neurons preferentially respond to high frequency stimulations, while tonic spiking neurons preferentially respond to low and middle frequency stimulations.[2,8] Recently, identifying the dynamics and functions of class-3 excitability or phasic spiking modulated by various modulation measures has attracted increasing attention.[5,8–10]

Electrophysiological experiments have demonstrated that many types of neurons in nervous systems exhibit phasic spiking, such as auditory brainstem neurons,[8,11] vasopressin neurons,[12] and Grueneberg ganglion olfactory neurons.[13] Phasic spiking neurons show extraordinary temporal precision and coincidence detection in response to excitatory inputs,[11] which contributes to the sound localization of the auditory brainstem. The transitions between tonic spiking and phasic spiking have been found in the development of the auditory cortex.[14] These transitions are related to vocal learning and memory. To reveal the dynamics of distinct spiking patterns and spike initiating dynamics, we utilize the theory of nonlinear dynamics,[5,15] such as the bifurcation and threshold (separatrix or quasi-separatrix) curve of the action potential in the phase plane. For example, the change from the resting state to repetitive spiking via a saddle-node on an invariant circle bifurcation corresponds to class-1 excitability, and Hopf bifurcation corresponds to class-2 excitability.[7] The resting state is stable and no bifurcation related to the stable limit cycle occurs, which corresponds to class-3 excitability.[7] Furthermore, the phase trajectory of spiking behavior induced from the resting state can be well understood with a separatrix or quasi-separatrix curve in the phase plane.[5,16,17] For example, the all-or-none spikes associated with class-1 excitability[16] and phasic spiking associated with class-3 excitability can be interpreted by determining whether the trajectory perturbed by external stimulation can cross over the separatrix curve (stable manifold of the saddle) or quasi-separatrix curve.[5]

The firing activities of a neuron such as the transition between tonic spiking and phasic spiking can be modulated with synaptic inputs in addition to the intrinsic dynamics of the

†Corresponding author. E-mail: zzg164637758@163.com

© 2022 Chinese Physical Society and IOP Publishing Ltd

neuron.[10,18] In the general view, synaptic inhibition hyperpolarizes membrane potential away from the spike threshold to reduce spiking activity, which differs from synaptic excitation that depolarizes membrane potential across the spike threshold to enhance spiking activity.[19] For example, synaptic inhibition causes subtractive and divisive effects that reduce the neuronal firing rate.[20,21] However, some studies have shown different points of view. For instance, inhibitory current can induce a spike from the resting state near the Hopf point, which is based on the mechanism of post-inhibitory rebound (PIR) spike.[16,22] PIR spike has been observed in multiple types of neurons, such as hippocampal pyramidal neurons,[15] neocortex neurons,[23] entorhinal cortex pyramidal neurons, interneurons,[22,24,25] and auditory brainstem neurons,[26] and PIR spike is associated with many cellular and physiological functions.[22,24–26] For instance, PIR spike aroused by precisely timed inhibition can promote the spatial sensitivity of auditory systems to faint sounds.[27,28] Superior paraolivary nucleus neurons in the auditory brainstem can encode sinusoidally amplitude-modulated tones with PIR spike. The robustness of synchronous oscillations in an inhibitory interneuronal network can enhance the PIR spike.[23] For the resting state corresponding to stable focus, the subthreshold inhibitory synaptic input preceding the subthreshold excitatory synaptic input can facilitate the elicitation of a spike induced by the excitatory input,[19] which is called post-inhibitory facilitation (PIF) and has been observed in the electrophysiological experiment for brainstem auditory neurons.[29]

In addition to synaptic inputs from other neurons, a neuron may receive synaptic inputs from itself; i.e., a neuron may receive self-feedback from an autapse, which is a special synapse that connects the dendrite and axon of the neuron.[30] Autapses have been found in many kinds of neurons, including neocortical interneurons, pyramidal neurons,[31] cerebellar interneurons,[32] hippocampal interneurons,[33] and olfactory bulb neurons.[34] Electrophysiological experiments have identified that autapses play critical roles in the firing activities of single neurons[33–36] and network synchronizations.[37] For example, inhibitory autapse inhibits the firing activities[35] and increases the precision of spike timing in neocortical interneurons.[36] Excitatory autapses cause persistent firing in the motor neurons of buccal ganglia[34] and enhance burst firing in neocortical pyramidal neurons.[31] In addition, researchers have presented more roles for autapses in modulating the activities of single neurons and neuronal networks such as firing patterns,[18,38,39] resonances,[40–42] and synchronizations[43,44] in theoretical studies.[45–47] For example, the switches between class-1 and 2 excitabilities can be induced by inhibitory and excitatory autapses. Inhibitory autapse usually suppresses burst firing while excitatory autapse enhances burst firing.[39,48] In particular, recent research has shown some paradoxical results for the inhibitory and excitatory autapses, which can enhance and reduce neuronal firing, respectively. Specifically, excitatory autapse can reduce the spike number of a bursting neuron[49] and change from repetitive spiking near the subcritical Hopf bifurcation (corresponds to class-2 excitability) to the resting state or mixed-mode oscillations.[50] Inhibitory autapse can enhance the spike number of bursting patterns[51] and change the resting state near the Hopf bifurcation as repetitive spiking by modulating the time delay in the inhibitory autapse.[52] These results extended knowledge on functions of inhibitory and excitatory autapses that can modulate neuronal firing patterns or frequencies to encode information.

As determined by reviewing the literature, it is well known that an inhibitory current pulse can induce PIR spike for class-2 excitability corresponding to Hopf bifurcation.[16] Based on this, the promotion effect of the inhibitory autapse on the spiking activities of neurons with class-2 excitability has been found and interpreted.[23,52] Recently, the PIF phenomenon has been simulated for both class-2 excitability and class-3 excitability.[19,53] Compared with class-2 excitability, there are fewer reports about the PIR spike and enhancement of spiking activity induced by the inhibitory effect for class-3 neurons.[7,8] In this study, the effects of an inhibitory autapse with time delay on dynamical behaviors of the Morris–Lecar (ML) neuron with class-3 excitability are investigated. The quasi-separatrix curve[5] (threshold of action potential) exhibits a shape resembling that of class-2 excitability. Therefore, it is found that an inhibitory current pulse can induce a PIR spike, and this depends on whether the inhibitory pulse can push the trajectory to run across the quasi-separatrix curve in the phase plane. This result presents the dynamical mechanism of a PIR spike for a class-3 neuron. Furthermore, we simulate the phasic spiking changing to tonic spiking in a class-3 neuron with an inhibitory autapse, which shows that the inhibitory autapse enhances the firing activity. The tonic spiking is explained by the PIR spike mechanism. The threshold curve for autaptic conductance to induce the transition with respect to the time delay exhibits a period approximating the period of afterpotentials of phasic spiking. We discuss the difference between this study and a recent research in which the phasic spiking[18] remains unchanged for a class-3 neuron with inhibitory autapse. The result presents a potential function for an inhibitory autapse that modulates the firing activities of a class-3 neuron and extends the paradoxical effects of an inhibitory autapse that can enhance neuronal firing.

The rest of the paper is organized as follows: The model of an ML neuron with an inhibitory autapse is given in Section 2. In Section 3, the dynamical mechanism of the hyperpolarizing-current-pulse-induced PIR spike for the class-3 ML neuron is given, and the changes from tonic spiking to

phasic spiking induced by inhibitory autapse are presented. The discussion and conclusion are given in Section 4.

2. Models

2.1. Model of the isolated class-3 ML neuron

The modified Morris–Lecar (ML) model,[5] which is a conductance-based model and can simulate three classes of excitability by varying one single parameter, is generally used to study the effects of different classes of excitabilities on neuronal responses to external stimulations, including synaptic inputs and noise as well as network synchronizations. The current balance equation of an ML neuron is described as

$$C\dot{V} = -I_{\rm K} - I_{\rm Na} - I_{\rm L} + I_{\rm DC}, \tag{1}$$

where V represents the membrane potential, C is the membrane capacitance, and $I_{\rm DC}$ is the constant depolarization current. $I_{\rm L} = \bar{g}_{\rm L}(V - E_{\rm L})$, $I_{\rm Na} = \bar{g}_{\rm Na} m_\infty(V)(V - E_{\rm Na})$, and $I_{\rm K} = \bar{g}_{\rm K} w(V - E_{\rm K})$ are the leakage, sodium, and delayed rectifier potassium currents, respectively, where $E_{\rm L}$ ($E_{\rm Na}$ and $E_{\rm K}$) and $\bar{g}_{\rm L}$ ($\bar{g}_{\rm Na}$ or $\bar{g}_{\rm K}$) are the reversal potential and maximum conductance of $I_{\rm L}$ ($I_{\rm Na}$ or $I_{\rm K}$). The activation of $I_{\rm Na}$ is dependent on the steady-state function $m_\infty(V) = 0.5\{1 + \tanh[(V - \beta_m)/\gamma_m]\}$. The variable w is the activation variable of $I_{\rm K}$ and it is determined by

$$\dot{w} = \phi_{\rm w}(w_\infty(V) - w)/\tau_{\rm w}(V), \tag{2}$$

where the related expressions of $\tau_{\rm w}(V)$ and $w_\infty(V)$ are $\tau_{\rm w}(V) = \cosh^{-1}[(V - \beta_{\rm w})/2 \cdot \gamma_{\rm w}]$ and $w_\infty(V) = 0.5\{1 + \tanh[(V - \beta_{\rm w})/\gamma_{\rm w}]\}$.

The parameter values of the model are set as follows: $C = 2$ μF/cm^2, $\bar{g}_{\rm Na} = 20$ ms/cm^2, $E_{\rm Na} = 50$ mV, $\beta_m = -1.2$ mV, $\gamma_m = 18$ mV, $\bar{g}_K = 20$ ms/cm^2, $E_{\rm K} = -100$ mV, $\gamma_{\rm w} = 10$ mV, $\phi_{\rm w} = 0.15$, $g_{\rm L} = 2$ ms/cm^2, and $E_{\rm L} = -70$ mV. The excitability of the ML neuron can be changed as $\beta_{\rm w}$ varies.[5,54] When $\beta_{\rm w} = -25$ mV, the ML neuron can exhibit class-3 excitability. Unless otherwise stated, the model is called the isolated class-3 ML neuron model. The bifurcation diagrams are numerically computed using XPPAUTO.[55]

2.2. Model of the inhibitory autaptic class-3 ML neuron

To study the effects of inhibitory autapse on neuron with class-3 excitability, an inhibitory autaptic current $I_{\rm aut}$ is introduced to the right-hand side of the current balance equation (1):

$$C\dot{V} = -I_{\rm Na} - I_{\rm K} - I_{\rm L} + I_{\rm DC} - I_{\rm aut}, \tag{3}$$

the inhibitory autaptic current is given by

$$I_{\rm aut} = g_{\rm aut} s(V - E_{\rm syn}), \tag{4}$$

where $E_{\rm syn}$ and $g_{\rm aut}$ denote the reversal potential and the maximum conductance of the inhibitory autapse, respectively, and s is the activation variable of the inhibitory autapse, determined by

$$\dot{s} = \alpha\Gamma(V(t - \tau))(1 - s) - \beta s. \tag{5}$$

Here, α and β are the raising and decaying rates, which are set as 12 ms^{-1} and 1 ms^{-1}, respectively. $\Gamma(V(t - \tau)) = 1/(1 + \exp(-10(V(t - \tau) - \theta_{\rm thres})))$, with τ being the time delay in the autapse, and $\theta_{\rm thres} = -15$ mV the autaptic threshold for which autaptic current is triggered by an upstroke of the actional potential passing through it. The parameter $E_{\rm syn}$ is set to -80 mV for the inhibitory autapse. The model is called the inhibitory autaptic class-3 ML neuron.

The models are integrated numerically using the Runge–Kutta method with steps of 0.01 ms.

3. Results

3.1. Dynamics for phasic spiking of the isolated class-3 ML neuron

For the isolated class-3 ML neuron, the equilibrium (corresponding to the resting state) is stable focus (black line), no bifurcation or stable limit cycle (corresponding to repetitive spiking) appears with the increase of the constant depolarizing current $I_{\rm DC}$, as shown in Fig. 1(a). If $I_{\rm DC}$ is fixed at 80 μA/cm^2, when a subthreshold depolarization current pulse $I_{\rm pulse} = 20$ μA/cm^2 (100-ms duration, green curve in bottom panel of Fig. 1(b) is applied to the ML neuron, subthreshold oscillations appearing at the onset of the depolarizing current pulse are induced, as shown in Fig. 1(b). When suprathreshold depolarizing current pulses $I_{\rm pulse} = 40$ μA/cm^2 (red) and $I_{\rm pulse} = 60$ μA/cm^2 (black) are applied to the ML neuron, only one spike is elicited at the onset of the depolarization current pulses, i.e., the ML neuron exhibits phasic spiking, as shown in the top two panels of Fig. 1(b). Both the subthreshold oscillations and the spike are transient behaviors.

Figures 1(c) and 1(d) show the trajectories corresponding to the behaviors in the second and third panels of Fig. 1(b), respectively. Before the stimulations of the depolarization current pulse $I_{\rm pulse}$, the nullclines $\dot{V} = 0$ (gray dotted curve, corresponding to $I_{\rm DC} = 80$ μA/cm^2) and $\dot{w} = 0$ (gray dashed curve) intersect at a stable focus SE_1 (gray solid circle). During the processes of the stimulations ($I_{\rm pulse} = 20$ μA/cm^2 and $I_{\rm pulse} = 40$ μA/cm^2), the nullcline $\dot{V} = 0$ shifts upward, and the nullcline $\dot{w} = 0$ remains unchanged. The shifted nullcline $\dot{V} = 0$ (black dotted curves, $I_{\rm DC} = 120$ μA/cm^2 and $I_{\rm DC} = 100$ μA/cm^2) intersects with the nullcline $\dot{w} = 0$ at a new stable focus SE_2 (black solid circle). Under the perturbation of the depolarization current pulse, the trajectory moves from SE_1 to the new stable focus SE_2 via different paths, which

means that different transient behaviors appear at the onset of stimulation. If the intensity of the depolarizing current pulse is strong enough, for example, the depolarization current pulse $I_{\rm pulse} = 40\ \mu{\rm A/cm^2}$ can push the trajectory to cross over the quasi-separatrix curve (threshold of action potential) to form a spike, as shown in Fig. 1(c). If the intensity of the depolarization current pulse is weak, for example, the stimulation $I_{\rm pulse} = 20\ \mu{\rm A/cm^2}$ cannot push the trajectory to cross over the quasi-separatrix curve, resulting in subthreshold oscillations (Fig. 1(d)). The distinction between the spike and subthreshold oscillations appearing at the onset of the depolarizing current pulse is whether the current pulse can push the trajectory to cross over the quasi-separatrix curve or not. This indicates that the quasi-separatrix curve, which separates the phase plane into two regions with different behaviors, is an important factor that influences the spike elicitation. From the concave upward shape of the quasi-separatrix curve, the trajectory starting from the equilibrium may run across the left part of the quasi-separatrix curve under the action of the hyperpolarization current pulse with strong enough intensity, i.e., a PIR spike may be elicited.

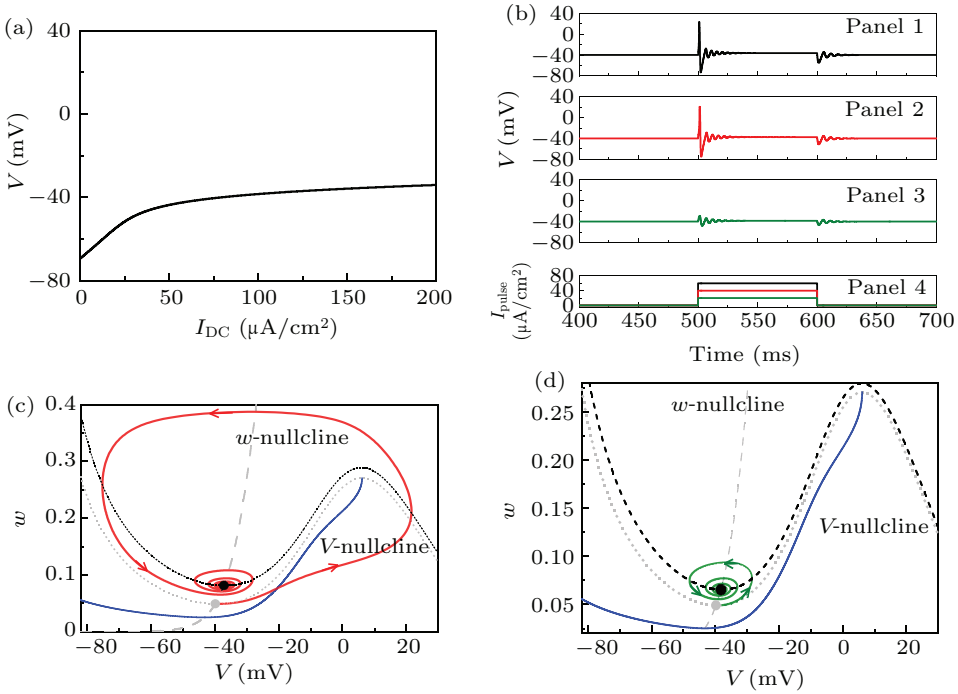


Fig. 1. Responses of the isolated class-3 ML neuron (Eqs. (1) and (2)) to depolarization stimulation at different levels. (a) The stable focus (equilibrium, black solid curve) changes with the increases of $I_{\rm DC}$. (b) The first, second, and third panels are, respectively, the potential responses of the isolated class-3 ML neuron (Eqs. (1) and (2)) to the depolarization current pulses of $I_{\rm pulse} = 60\ \mu{\rm A/cm^2}$ (black curve in the last panel), $I_{\rm pulse} = 40\ \mu{\rm A/cm^2}$ (red curve in the last panel), and $I_{\rm pulse} = 20\ \mu{\rm A/cm^2}$ (green curve in the last panel) when $I_{\rm DC} = 80\ \mu{\rm A/cm^2}$. (c) The trajectory corresponds to the behavior of the second panel in (b) on the phase plane (V, w). (d) The trajectory corresponds to the behavior of the third panel in (b) on the phase plane (V, w). The gray dashed and dotted curves are nullclines $\dot{w} = 0$ and $\dot{V} = 0$ when $I_{\rm DC} = 80\ \mu{\rm A/cm^2}$, respectively. The black dotted curves in (c) and (d) are nullcline $\dot{V} = 0$ for $I_{\rm DC} = 120\ \mu{\rm A/cm^2}$ and $100\ \mu{\rm A/cm^2}$, respectively. The gray solid circle is the stable equilibrium SE_1 when $I_{\rm DC} = 80\ \mu{\rm A/cm^2}$, the black circles in (c) and (d) are stable equilibria SE_2 when $I_{\rm DC} = 120\ \mu{\rm A/cm^2}$ and $100\ \mu{\rm A/cm^2}$, respectively. The blue curves in (c) and (d) are quasi-separatrix curves of the action potential when $I_{\rm DC} = 80\ \mu{\rm A/cm^2}$, respectively.

3.2. PIR spike induced by hyperpolarization current pulse and their dynamics

Based on the above phase plane analysis on the quasi-separatrix curve, a PIR spike can be simulated by applying a strong hyperpolarization current pulse to the class-3 ML neuron.

Figure 2 shows the responses of the class-3 ML neuron to the hyperpolarization current pulses with a brief duration when $I_{\rm DC} = 80\ \mu{\rm A/cm^2}$. A PIR spike is induced by the hyperpolarization current pulse $I_{\rm pulse} = -40\ \mu{\rm A/cm^2}$ with a 2-ms duration while it can not be induced by $I_{\rm pulse} = -20\ \mu{\rm A/cm^2}$ with the same duration, as shown in Figs. 2(a1) and 2(b1), respectively. Under the action of the hyperpolarization current pulse $I_{\rm pulse} = -40\ \mu{\rm A/cm^2}$, the trajectory (red solid line) moves to the left to run across the part of the quasi-separatrix curve left to the stable equilibrium point to form a spike (black solid line), as shown in Figs. 2(a2) and 2(a3). This is different from the depolarization current pulse, which pushes the trajectory across the part of the quasi-separatrix curve right to the stable equilibrium to form a spike (Fig. 1(c)). Under the action of the hyperpolarization current pulse $I_{\rm pulse} = -20\ \mu{\rm A/cm^2}$, the trajectory (red solid line) cannot pass through the quasi-separatrix curve to form subthreshold oscillations due to the fact that the hyperpolarization current pulse is weak, as shown in Figs. 2(b2) and 2(b3).

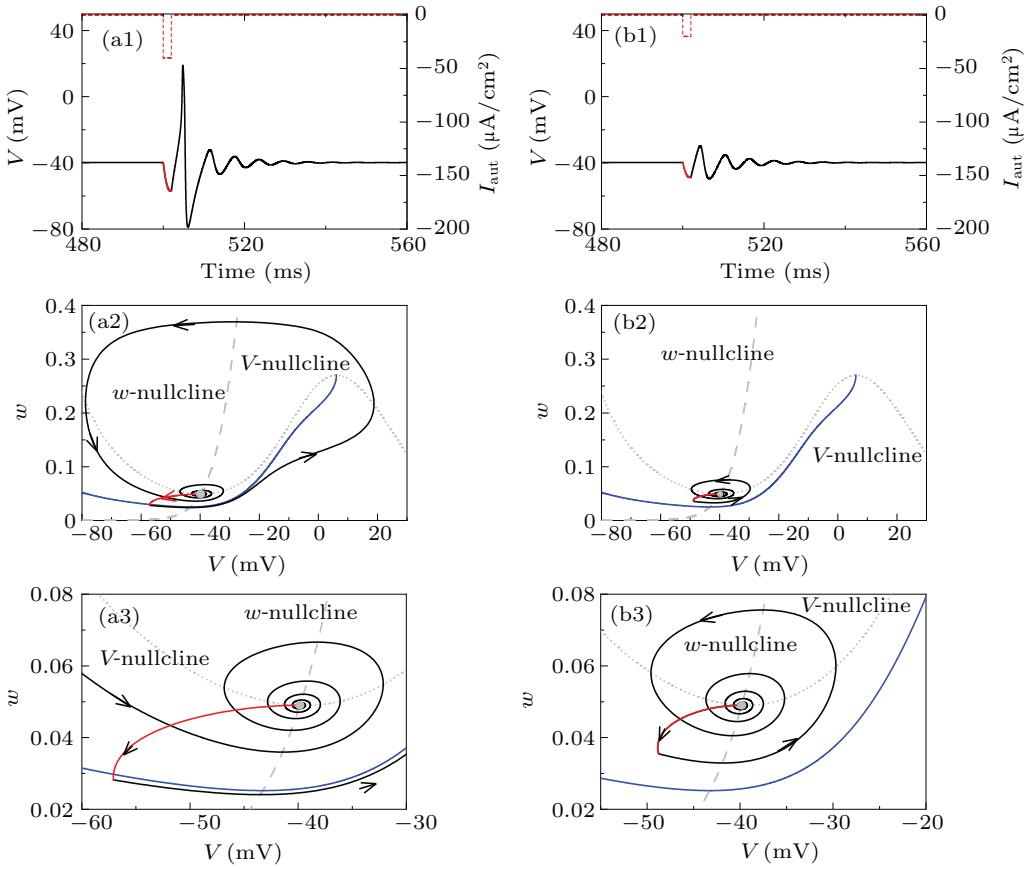


Fig. 2. Dynamics of PIR spike induced by hyperpolarization current pulse for the isolated class-3 ML neuron (Eqs. (1) and (2)) when $I_{DC} = 80\ \mu A/cm^2$. (a1) PIR spike when $I_{pulse} = -40\ \mu A/cm^2$. (b1) PIR when $I_{pulse} = -20\ \mu A/cm^2$. The red dashed curve is the hyperpolarization current pulse. The black solid curve and the red solid curve are the membrane potential, and the red solid part is the membrane potential under the action of the hyperpolarization current pulse. (a2) The phase trajectory corresponds to (a1). The black and red parts correspond to the black and red solid parts in (a1), respectively. (b2) The phase trajectory corresponds to (b1). The black and red parts correspond to the black and red solid parts in (b1), respectively. (a3) Enlargement of (a2). (b3) Enlargement of (b2). The blue solid curve is the quasi-separatrix curve. The gray dashed and dotted curves are nullclines $\dot{w} = 0$ and $\dot{V} = 0$, respectively. The duration of both current pulses is 2 ms.

3.3. Tonic spiking induced by inhibitory autapse and their dynamics

This subsection describes how the tonic spiking is induced by the inhibitory autapse with time delay for the class-3 ML neuron. For the isolated class-3 ML neuron, the stable behavior is the resting state (corresponding to equilibrium), and no stable repetitive spiking (corresponding to the limit cycle) exists when I_{DC} is within the physiological range (Fig. 1(a)). If the initial values of the model are chosen in the region below the quasi-separatrix curve in the phase plane (V, w), the isolated ML neuron exhibits phasic spiking. For example, the phasic spiking followed by subthreshold oscillations (green line) is shown in Fig. 3(a) ($I_{DC} = 80\ \mu A/cm^2$).

When the inhibitory conductance $g_{aut} = 3.0\ ms/cm^2$ and time delay $\tau = 3$ ms are fixed in the inhibitory autaptic class-3 ML neuron model, the autapse can induce the phasic spking changing to tonic spiking (black and red solid lines), as shown in Figs. 3(a) and 3(b). The inhibitory autaptic current (red dashed line) exhibits a pulse shape. The first inhibitory autaptic current pulse (red dashed line) in Figs. 3(a) and 3(b) delays 3 ms from the first spike (black solid line), causing that the first pulse of the inhibitory autaptic current acts at the after-hyperpolarization phase to induce the second spike (the red solid curve). The inhibitory autaptic current has a significantly inhibitory effect on membrane potential, which can induce a PIR spike (the second spike). From Figs. 3(c) and 3(d), the inhibitory autaptic current pulse can push the trajectory (red solid curve) across the quasi-separatrix curve (blue solid curve) to form the second spike. The inhibitory autaptic current after the pulse (around the second spike) is weak, its action is relatively small, hence, the amplitude of the second spike is slightly smaller than that of the first spike. The next delayed autaptic current pulse can evoke the third spike, then the fourth spike and so on. Tonic spiking is induced by the inhibitory autapse from phasic spiking.

3.4. Dependence of tonic spiking on autaptic conductance and time delay

As shown in Fig. 3, the autaptic conductance and time delay may determine whether the inhibitory autaptic current can push the trajectory across the quasi-separatrix curve to form a spike. To present the effects of them on repetitive spiking generation, the distributions of the phasic spiking and tonic spik-

ing on the parameter plane $(\tau, g_{\rm aut})$ when $I_{\rm DC} = 75$ μA/cm^2, $I_{\rm DC} = 80$ μA/cm^2, $I_{\rm DC} = 85$ μA/cm^2 and $I_{\rm DC} = 90$ μA/cm^2 are shown in Figs. 4(a)–4(d), where the firing frequency of tonic spiking is symbolized by different color scales. From Fig. 4, we can find the following three characteristics:

(1) The region of tonic spiking appears on the top right corner of $(\tau, g_{\rm aut})$ in each panel, which indicates that the inhibitory autapse has strong conductance and a long time delay.

(2) The border between the regions of tonic and phasic spiking exhibits oscillations as τ increases, which is similar to the damped oscillations (green curve) after the phasic spiking in Fig. 3(a). For example, when $I_{\rm DC} = 85$ μA/cm^2, three local minima of the boundary appear at $\tau \approx 4.71$ ms, $\tau \approx 11.04$ ms, and $\tau \approx 17.14$ ms. The difference between two successive time delays is ~ 6.2 ms, which approximately equals the time difference (~ 6.25 ms) of two successive minima of damped oscillations shown in Fig. 3(a).

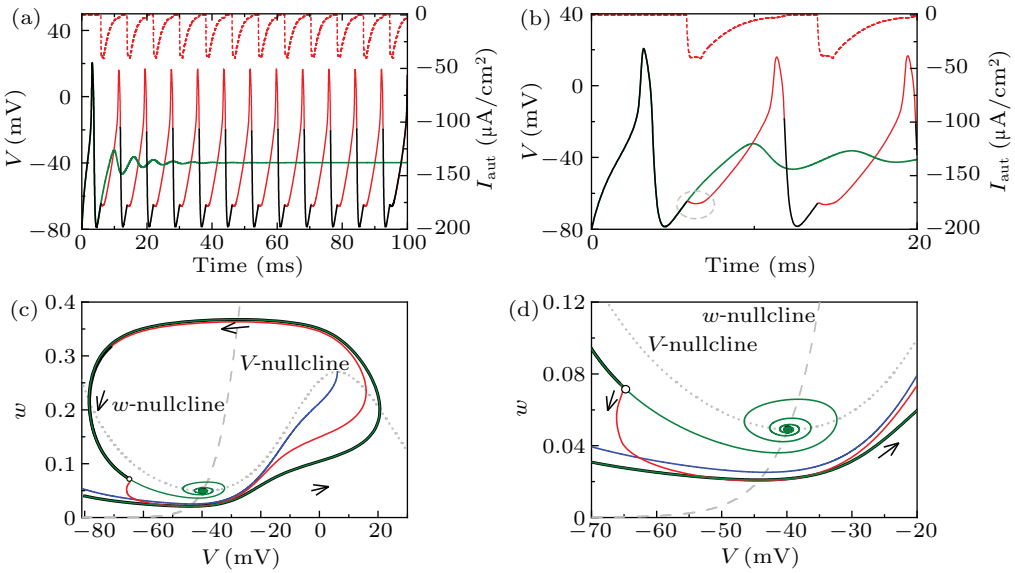


Fig. 3. Inhibitory-autapse-induced tonic spiking for the inhibitory autaptic class-3 ML neuron (Eqs. (3)–(5)). (a) Spike train. The red and black solid curves are the membrane potentials of the inhibitory autaptic class-3 ML neuron (Eqs. (3)–(5)). The red dashed curve is the autaptic current. The green solid curve is the membrane potential of the isolated class-3 ML neuron (Eqs. (1) and (2)). (b) Enlarged view of (a). (c) The tonic spiking induced by the inhibitory autapse for (a). The red, black, and green solid curves are the trajectories corresponding to the membrane potential labeled by the same color scheme. The gray dashed and dotted curves are the nullclines $\dot{w} = 0$ and $\dot{V} = 0$ for the isolated class-3 ML neuron (Eqs. (1) and (2)). The blue curve is a quasi-separatrix curve (Eqs. (1) and (2)). The black solid circle denotes the stable focus. The black hollow circle is the initial phase of the inhibitory autaptic current. (d) Enlargement of (c). Parameter values: $g_{\rm aut} = 3.0$ ms/cm^2, $\tau = 3$ ms, and $I_{\rm DC} = 80$ μA/cm^2.

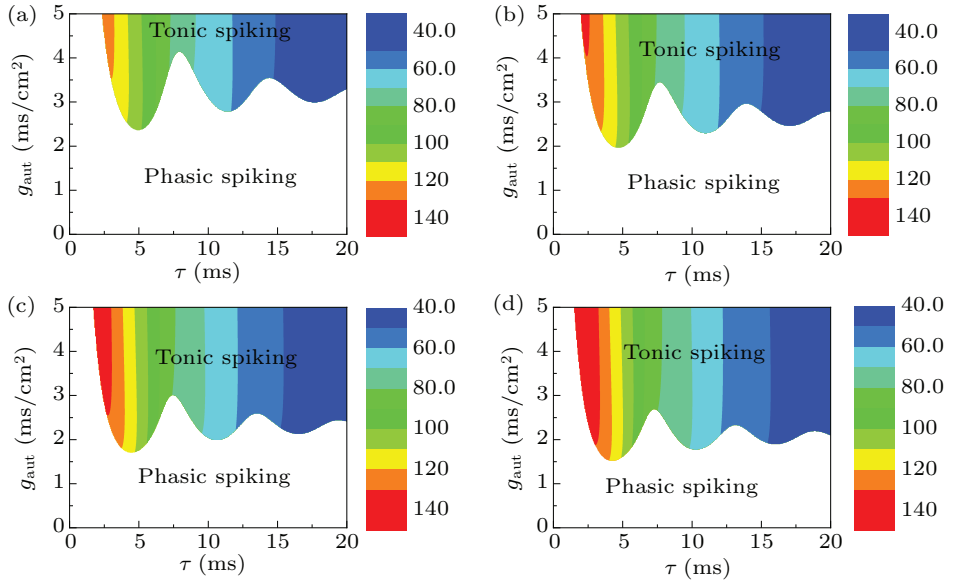


Fig. 4. Effect of the autaptic conductance and time delay on the dynamical behaviors for the inhibitory autaptic class-3 ML neuron (Eqs. (3)–(5)) when $I_{\rm DC}$ is fixed as different values. (a) $I_{\rm DC} = 75$ μA/cm^2; (b) $I_{\rm DC} = 80$ μA/cm^2; (c) $I_{\rm DC} = 85$ μA/cm^2; (d) $I_{\rm DC} = 90$ μA/cm^2. The behaviors in the blank and colorful regions are phasic spiking and tonic spiking, respectively. The color bar represents the firing frequency of the tonic spiking.

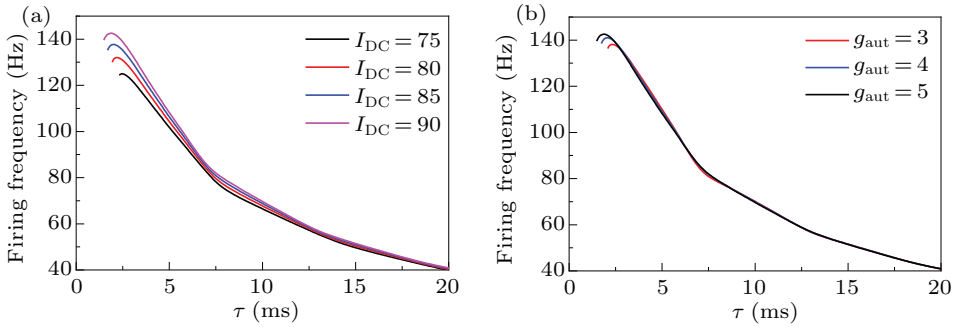


Fig. 5. The changes in the firing frequency with respect to time delay for the inhibitory autaptic class-3 ML neuron (Eqs. (3)–(5)). (a) For different I_{DC} when $g_{aut} = 5.0$ ms/cm^2, where $I_{DC} = 75$ μA/cm^2 (black), 80 μA/cm^2 (red), 85 μA/cm^2 (blue), and 90 μA/cm^2 (magenta). (b) For different g_{aut} when $I_{DC} = 90$ μA/cm^2, where $g_{aut} = 3.0$ ms/cm^2(red), 4.0 ms/cm^2(blue), and 5.0 ms/cm^2(black).

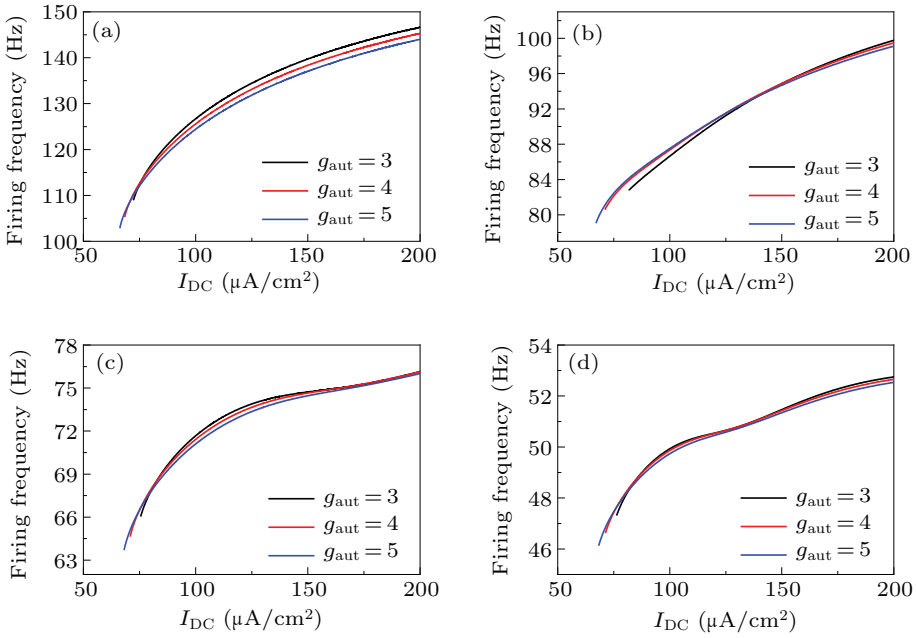


Fig. 6. For the inhibitory autaptic class-3 ML neuron (Eqs. (3)–(5)), the firing frequency of tonic spiking varies with I_{DC} at three autaptic conductances g_{aut} when τ is fixed as different values: (a) $\tau = 4$ ms, (b) $\tau = 7$ ms, (c) $\tau = 10$ ms, (d) $\tau = 16$ ms. Other parameters are $g_{aut} = 3$ ms/cm^2 (black), 4 ms/cm^2 (red), and 5 ms/cm^2 (blue).

(3) The larger the time delay is, the smaller the firing frequency of the tonic spiking is. To obtain more details, the changes in the firing frequency with respect to τ for different I_{DC} ($g_{aut} = 5.0$ ms/cm^2) are shown in Fig. 5(a), and those for different g_{aut} ($I_{DC} = 90$ μA/cm^2) are shown in Fig. 5(b). With the increases of τ, the firing frequency mainly decreases (Figs. 5(a) and 5(b)), except for a very narrow range when the time delay is small.

The distinctions among the different panels of Fig. 4 exhibit two characteristics:

(1) The threshold g_{aut} for tonic spiking decreases as I_{DC} increases, which indicates that it is easier for the inhibitory autapse to induce tonic spiking for the larger I_{DC}.

(2) The firing frequency increases as I_{DC} increases. To present the changes, the firing frequencies of the tonic spiking changing with I_{DC} for different g_{aut} when $\tau = 4$ ms, $\tau = 7$ ms, $\tau = 10$ ms, and $\tau = 16$ ms are shown in Figs. 6(a)–6(d). It should be noted that the firing frequency monotonously increases from a nonzero value.

3.5. Dependence of tonic spiking induced by inhibitory autapse on β_w

In addition to the autaptic conductance and time delay of the inhibitory autapse, the intrinsic parameters of the isolated class-3 ML model may also have great influence on inhibitory autapse to induce the tonic spiking. In the isolated class-3 ML model, β_w is an important parameter that determines neuronal excitability and firing pattern of the isolated ML neuron. For example, the distribution of the class-2 excitability, class-3 excitability (phasic spiking), and tonic spiking on parameter plane (I_{DC}, β_w) is given in Fig. 7(a). The Hopf bifurcation curve (Hopf) and the saddle node bifurcation curve of the limit cycles (SNLC) on (I_{DC},β_w) are represented by the red curve and the black curve, respectively. The detailed bifurcations of the ML neuron model on (I_{DC},β_w) can refer to Ref. [54]. As can be seen from Figs. 7(a) and 7(b), the bifurcation curves Hopf and SNLC appear above $\beta_w = -24$ mV (gray dashed horizontal line), and no bifurcation appears below $\beta_w = -24$ mV. Upwards of $\beta_w = -24$ mV (gray dashed

horizontal line), class-2 excitability and tonic spiking appear on the left and right of the SNLC (black curve), respectively. Lower than the curve $\beta_w = -24$ mV (gray dashed horizontal line), the behavior is class-3 excitability (phasic spiking). When β_w is fixed at a value larger than -24 mV, tonic spiking is generated via the Hopf/SNLC bifurcation as I_{DC} increases, which appears in the upper right region above the SNLC curve. When β_w is fixed at a value smaller than -24 mV, only phasic spiking can be generated.

To present the effect of β_w on the tonic spiking when $\tau = 4$ ms, the distributions of the tonic spiking and phasic spiking on (I_{DC}, β_w) for different g_{aut} are shown in Figs. 7(b)–7(f). The firing patterns in the colorful and blank regions are tonic spiking and phasic spiking, respectively. The color scale represents the firing frequency of the tonic spiking. The border between the tonic spiking and phasic spiking corresponds to the SNLC (black curve) when $g_{aut} = 0$ ms/cm^2, as shown in each panel of Fig. 7, which is compared with the border of the phasic spiking and tonic spiking at different $g_{aut} > 0$. Several characteristics can be found from Figs. 7(b)–7(f).

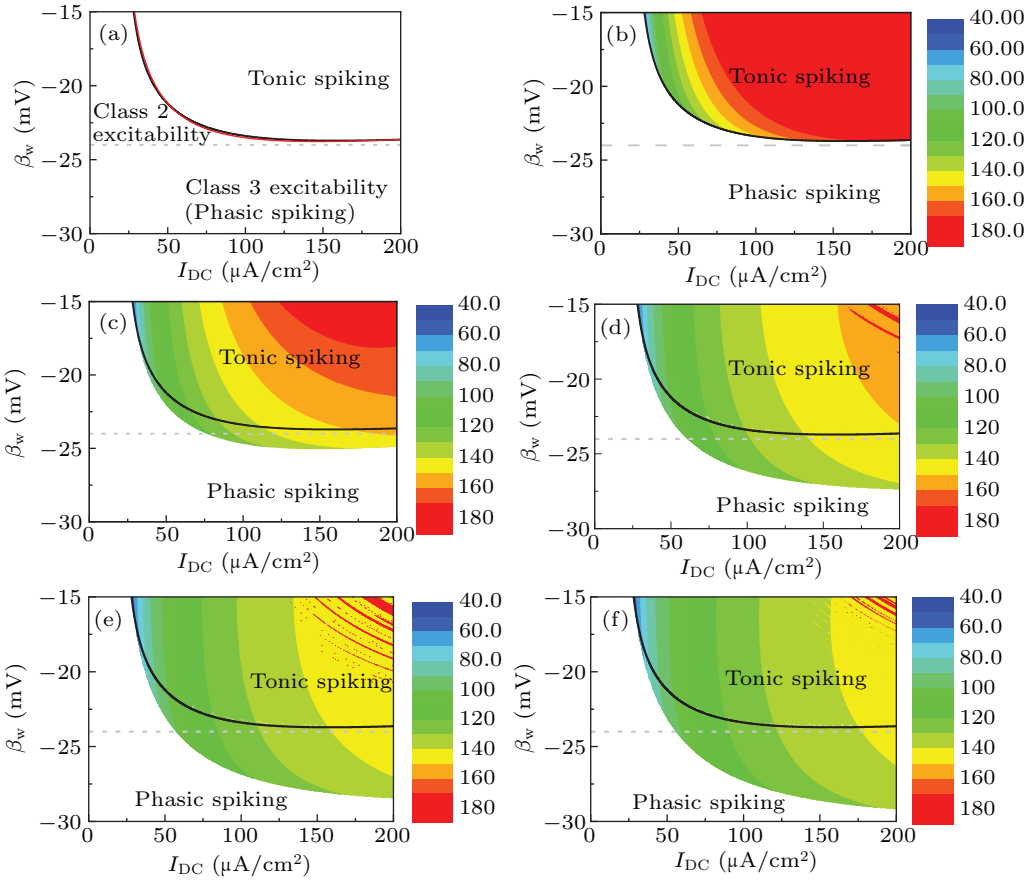


Fig. 7. Effect of β_w and I_{DC} on the tonic spiking induced by the inhibitory autapse at different g_{aut} values. (a) Bifurcation curves on the plane (I_{DC},β_w) of the isolated class-3 ML neuron model (Eqs. (1) and (2)). The red curve is the Hopf bifurcation (Hopf), the black curve is saddle node bifurcation of the limit cycles (SNLC), and the gray dashed curve is the boundary between the class-2 and 3 excitabilities. (b) Distribution of different firing patterns for the inhibitory autaptic class-3 ML neuron (Eqs. (3)–(5)) when $g_{aut} = 0$ ms/cm^2. (c)–(f) Distribution of different firing patterns for the inhibitory autaptic class-3 ML neuron (Eqs. (3)–(5)) when $g_{aut} = 1.0$ ms/cm^2, $g_{aut} = 3.0$ ms/cm^2, $g_{aut} = 5.0$ ms/cm^2 and $g_{aut} = 7.0$ ms/cm^2, respectively. The behaviors in blank and colorful regions are phasic spiking and tonic spiking, respectively. The black curve and gray dashed curve are the bifurcation curve and boundary of the class-2 and 3 excitabilities in (a), respectively. The color bar represents the firing frequency of the tonic spiking. Other parameter: $\tau = 4$ ms.

(1) The phasic spiking near SNLC (black curve) in Fig. 7(b) is changed to tonic spiking (Figs. 7(c)–7(f)), which indicates that the inhibitory autapse can induce tonic spiking when β_w (phasic spiking corresponding to class-3 excitability) is close to the region (tonic spiking corresponding to class-2 excitability), i.e., β_w influences the change in the firing pattern induced by the inhibitory autapse.

(2) The region of the tonic spiking below the black curve in Figs. 7(c)–7(f) enlarges with the increase of g_{aut}. The larger the g_{aut} is, the smaller the critical value of β_w for the phasic spiking is.

(3) The firing frequency of the tonic spiking below the black curve in Figs. 7(c)–7(f) increases with the increase of I_{DC} or β_w. To obtain more details, the changes in the firing frequency when $I_{DC} = 75$ μA/cm^2 and $I_{DC} = 90$ μA/cm^2, are shown in Figs. 8(a) and 8(b), respectively, and the firing frequency increases monotonously with the increase of β_w.

When $\beta_w = -24$ mV and $\beta_w = -28$ mV, the firing frequency-I_{DC} curves are shown in Figs. 8(c) and 8(d), respectively. With the increase of I_{DC}, the firing frequency initi-

ates from a certain nonzero value and increases continuously, which exhibits the characteristics of class-2 excitability. Compared with Fig. 1(a), no bifurcation occurs with respect to I_{DC}. Figures 8(c) and 8(d) indicate that the introduction of the inhibitory autapse can induce the change in neuronal excitability from class 3 to class 2. The change induced by the inhibitory autapse is different from that induced by other outward ("negative") currents such as M-type potassium currents because the activation is suprathreshold for the inhibitory autaptic current and subthreshold for the other outward ion currents.[5,6]

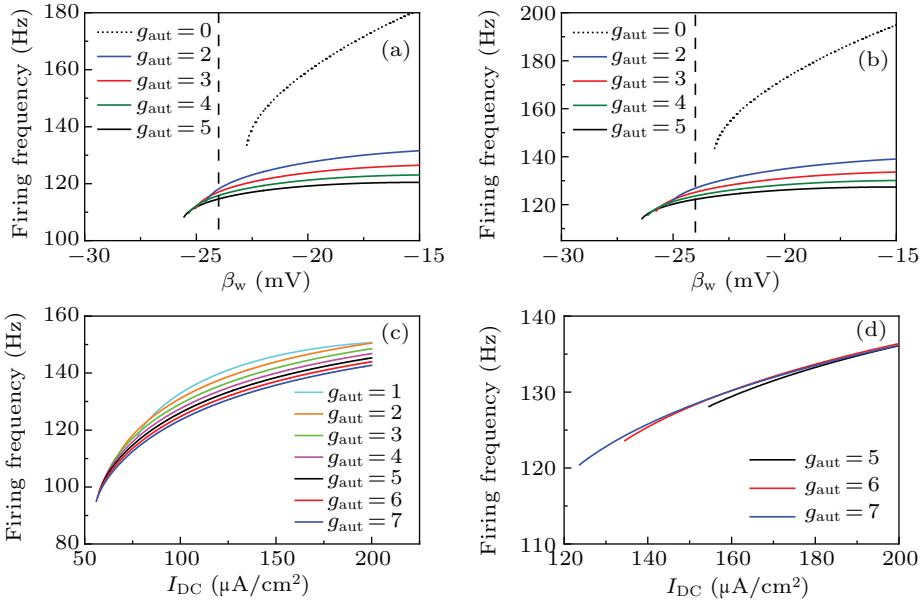


Fig. 8. Effects of β_w and I_{DC} on the firing frequency of tonic spiking induced by inhibitory autapse for the inhibitory autaptic class-3 ML neuron (Eqs. (3)–(5)). (a) and (b) The firing frequency varies with β_w for different g_{aut} when $I_{DC} = 75$ μA/cm^2 and $I_{DC} = 90$ μA/cm^2, respectively. The vertical dashed line ($\beta_w = -24$ mV) is the boundary between the class-2 and 3 excitabilities for the ML neuron. Class 3 excitability is on the left and class-2 excitability is on the right. The dotted curve is the firing frequency curve for the isolated class-3 ML neuron (Eqs. (1) and (2)). The solid curves labeled by different colors are the firing frequency curves for the inhibitory autaptic class-3 ML neuron (Eqs. (3)–(5)). (c) and (d) The firing frequency curves with I_{DC} for different g_{aut} when $\beta_w = -24$ mV and $\beta_w = -28$ mV, respectively. The solid curves labeled with different colors are the firing frequency curves for different g_{aut}. Other parameter: $\tau = 4$ ms.

4. Discussion and conclusion

PIR spike is an important characteristic of many neurons related to many cellular functions[24,26,56,57] and has been identified in class-2 excitability,[7,16] which presents one alternative way for inhibitory inputs to induce action potentials rather than excitatory inputs. The inhibitory inputs usually suppress the firing activities of neurons.[22] In this study, the PIR spike and transition from phasic spiking to tonic spiking induced by an inhibitory autapse for the class-3 ML neuron are acquired. Based on the basic view that class-3 excitability is far away from bifurcation, and the neuron exhibits phasic spiking behavior (i.e., damping oscillations with an intrinsic period following one or few spikes), the results show their significance in the following aspects.

Firstly, the condition for the PIR spike is extended to class-3 excitability. In the previous studies on theoretical models and experiments, the PIR spike has been identified to be elicited near subcritical Hopf bifurcation for class-2 neurons. Based on the characteristics of the PIR spike of class-2 neurons, a contour-intuitive phenomenon, in which repetitive spiking is evoked from the resting state near Hopf bifurcation by an inhibitory autapse with suitable time delay and autaptic conductance, is presented. Recently, a PIR spike has been identified to be evoked near saddle-node bifurcation on an invariant cycle (SNIC) or big Homoclinic bifurcation point for class-1 excitability.[58] All these results show that the PIR spike can be evoked near a bifurcation point. A recent study shows PIF of class-3 neuron, where inhibition preceding excitation can promote the membrane potential to the threshold of action potential, but whether inhibition can induce the PIR spike is unknown.[53] In this study, the PIR spike is identified to be elicited for class-3 excitability that is far from the bifurcation point, which extends the condition for the PIR spikes. This result is consistent with an electrophysiology experiment wherein the PIR spike can be induced in phasic spiking neurons[8] such as caudal mesopallium neurons. Furthermore, the occurrence of the PIR spike in the class-3 ML neuron depends on whether the inhibitory current pulse can push the trajectory to run across the quasi-separatrix curve (threshold of action potential) or not. If the inhibitory current pulse can push the trajectory to run across the quasi-separatrix curve, a PIR spike is elicited. The result presents a dynamical mechanism of the PIR spike for class-3 excitability, which provides a deep understanding of class-3 excitability.

Secondly, the condition for the counterintuitive nonlinear phenomenon in which the inhibitory effect can enhance neural

firing behavior is extended to class-3 excitability. In the previous studies, the counterintuitive phenomenon has been identified for class-2 excitability[52] and bursting behaviors.[51] For class-2 excitability, it is shown that inhibitory autapse can induce tonic spiking changing from resting state near Hopf bifurcation based on the PIR spike or cause an increase in the firing frequency of tonic spiking. For bursting neurons, it is shown that the inhibitory autapse can increase the spike number of burst firing. In this study, an inhibitory autapse with suitable conductance and time delay can induce tonic spiking (repetitive spiking) changing from phasic spiking that is far away from bifurcation, which extends the condition of paradoxical effect of inhibitory autapse. In a previous study, the phasic spiking remained unchanged after introducing an inhibitory autapse with time delay,[18] the reason may be that either the autaptic conductance is not strong enough or it has a slow decay rate. The result presents the potential function of class-3 neurons.

Thirdly, the threshold of the autaptic conductance to evoke tonic spiking exhibits oscillations with respect to time delay. The oscillation frequency of the threshold curve approximates that of the damping oscillations of the phasic spiking for class-3 excitability, and the difference between the minima of the threshold is close to the time difference between the minima of the damped oscillations after phasic spiking. When the autaptic conductance is larger than the threshold, the phasic spiking of the class-3 neuron activates a delayed, strong enough, and inhibitory autaptic current, which can push the trajectory near the stable focus to run across the quasi-separatrix curve and induce a PIR spike. The PIR spike reactivates the autaptic current and induces another delayed PIR spike. Repeating the above processes, a series of spikes are induced by the inhibitory autapse to form the tonic spiking, i.e., the inhibitory autapse induces the class-3 neuron changing from phasic spiking to tonic spiking. The result presents the dynamical mechanism for the enhanced spiking activity induced by the inhibitory autapse.

Lastly, class-3 neurons mediated by the inhibitory autapse exhibit distinct firing patterns such as phasic spiking and tonic spiking, which have different response properties that can affect neural processing.[1,2] For instance, when stimulated by broadband currents, phasic and tonic spiking neurons are tuned to higher and lower frequencies,[2,14] respectively. The distinct frequency preference between phasic and tonic neurons is useful for neurons to encode information at different timescales,[8] which may be related to some cellular functions. For example, phasic and tonic neurons in the auditory caudal mesopallium decode different frequency characteristics of songs and other vocalizations.[8] The result of the research shows a potential function of an inhibitory autapse that regulates the neuronal firing patterns related to neural encoding.

Acknowledgements

Project supported by the National Natural Science Foundation of China (Grant Nos. 11802085, 11872276, and 12072236), the Science and Technology Project of Guangzhou (Grant No. 202102021167), GDAS' Project of Science and Technology Development (Grant No. 2021GDASYL-20210103088), and the Science and Technology Development Program of Henan Province, China (Grant No. 212102310827).

References

[1] Bean B P 2007 *Nat. Rev. Neurosci.* **8** 451
[2] Ratté S, Hong S H, De Schutter E and Prescott S A 2013 *Neuron* **78** 758
[3] Hodgkin A L 1948 *J. Physiol.* **107** 165
[4] Hodgkin A L and Huxley A F 1952 *J. Physiol.* **117** 500
[5] Prescott S A, Koninck Y D and Sejnowski T J 2008 *PLoS Comput. Biol.* **4** e1000198
[6] Zhao Z G and Gu H G 2017 *Sci. Rep.* **7** 6760
[7] Izhikevich E M 2007 *Dynamical systems in neuroscience: The geometry of excitability and bursting* (Cambridge: MIT)
[8] Chen A N and Meliza C D 2018 *J. Neurophysiol.* **119** 1127
[9] Huguet G, Meng X Y and Rinzel J 2017 *Front. Comput. Neurosci.* **11** 3
[10] Zhao Z G, Li L and Gu H G 2020 *Sci. Rep.* **10** 3646
[11] Cook D L, Schwindt P C, Grande L A and Spain W J 2003 *Nature* **421** 66
[12] MacGregor D J and Leng G 2013 *PLoS Comput. Biol.* **9** e1003187
[13] Smith T C and Jahr C E 2002 *Nat. Neurosci.* **5** 760
[14] Chen A N and Meliza C D 2020 *J. Neurosci.* **40** 2047
[15] Prescott S A, Ratté S, De Koninck Y and Sejnowski T J 2008 *J. Neurophys.* **100** 3030
[16] Izhikevich E M 2000 *Int. J. Bifurcat. Chaos* **10** 1171
[17] Franci A, Drion G and Sepulchre R 2012 *SIAM J. App. Dyn. Syst.* **11** 1698
[18] Song X L, Wang H T and Chen Y 2019 *Nonlinear Dynam.* **96** 2341
[19] Dodla R and Rinzel J 2006 *Phys. Rev. E* **73** 010903
[20] Silver R A 2010 *Nat. Rev. Neurosci.* **11** 474
[21] Goldwyn J H, Slabe B R, Travers J B and Terman D 2018 *PLoS Comput. Biol.* **14** e1006292
[22] Ferrante M, Shay C F, Tsuno Y, Chapman G W and Hasselmo M E 2017 *Cereb. Cortex* **27** 2111
[23] Tikidji-Hamburyan R A, Martínez J J, White J A and Canavier C C 2015 *J. Neurosci.* **35** 15682
[24] Adhikari M H, Quilichini P P, Roy D, Jirsa V and Bernard C 2012 *J. Neurosci.* **32** 6501
[25] Shay C F, Ferrante M, Chapman IV G W and Hasselmo M E 2016 *Neurobiol Learn. Mem.* **129** 83
[26] Felix R A, Fridberger A, Leijon S, Berrebi A S and Magnusson A K 2011 *J. Neurosci.* **31** 12566
[27] Beiderbeck B, Myoga M H, Müller N I C, Callan A R, Friauf E, Grothe B and Pecka M 2018 *Nat. Commun.* **9** 1771
[28] Higgs M H, Kuznetsova M S and Spain W J 2012 *J. Neurosci.* **32** 15489
[29] Dodla R, Svirskis G and Rinzel J 2006 *J. Neurophys.* **95** 2664
[30] Van Der Loos H and Glaser E M 1972 *Brain Res.* **48** 355
[31] Bacci A, Huguenard J R and Prince D A 2003 *J. Neurosci.* **23** 859
[32] Bacci A and Huguenard J R 2006 *Neuron* **49** 119
[33] Yin L P, Zheng R, Ke W, He Q S, Zhang Y, Li J L, Wang B, Mi Z, Long Y S, Rasch M J, Li T F, Luan G M and Shu Y S 2018 *Nat. Commun.* **9** 4890
[34] Pouzat C and Marty A 1998 *J. Physiol.* **509** 777
[35] Cobb S R, Halasy K, Vida I, Nyiri G, Tamas G, Buhl E H and Somogyi P 1997 *Neuroscience* **79** 629
[36] Saada R, Miller N, Hurwitz I and Susswein A J 2009 *Curr. Biol.* **19** 479
[37] Manseau F, Marinelli S, Méndez P, Schwaller B, Prince D A, Huguenard J R and Bacci A 2010 *PLoS Biol.* **8** e1000492
[38] Uzun R, Yilmaz E and Ozer M 2017 *Physica A* **486** 386

[39] Guo D Q, Wu S D, Chen M M, Perc M, Zhang Y S, Ma J L, Cui Y, Xu P, Xia Y and Yao D Z 2016 *Sci. Rep.* **6** 26096
[40] Baysal V, Erkan E and Yilmaz E 2021 *Phil. Trans. R. Soc. A* **379** 20200237
[41] Uzun R 2017 *Appl. Math. Comput.* **315** 203
[42] Song X L, Wang H T and Chen Y 2018 *Nonlinear Dynam.* **94** 141
[43] Pinto M A, Rosso O A and Matias F S 2019 *Phys. Rev. E* **99** 062411
[44] Ge M Y, Jia Y, Xu Y, Lu L L, Wang H W and Zhao Y J 2019 *Appl. Math. Comput.* **352** 136
[45] Lin H R, Wang C H, Sun Y C and Yao W 2020 *Nonlinear Dynam.* **100** 3667
[46] Yao C G, He Z W, Nakano T, Qian Y and Shuai J W 2019 *Nonlinear Dynam.* **97** 1425
[47] Ren G D, Zhou P, Ma J, Cai N, Alsaedi A and Ahmad B 2017 *Int. J. Bifurcat. Chaos* **27** 1750187
[48] Wang H T, Ma J, Chen Y L and Chen Y 2014 *Commun. Nonlinear Sci. Numer. Simul.* **19** 3242
[49] Cao B, Gu H G and Li Y Y 2021 *Chin. Phys. B* **30** 050502
[50] Zhao Z G, Li L and Gu H G 2020 *Commun. Nonlinear Sci. Numer. Simul.* **85** 105250
[51] Li Y Y, Gu H G and Ding X L 2019 *Nonlinear Dynam.* **97** 2091
[52] Zhao Z G, Li L, Gu H G and Gao Y 2020 *Nonlinear Dynam.* **99** 1129
[53] Ma H Q, Jia B, Li Y Y and Gu H G 2021 *Neural Plast.* **2021** 6692411
[54] Liu C M, Liu X L and Liu S Q 2014 *Biol. Cybern.* **108** 75
[55] Ermentrout B 2002 *Simulating, analyzing, and animating dynamical systems: A guide to XPPAUT for researchers and students* (Philadelphia: SIAM) pp. 12–15
[56] Goaillard J M, Taylor A L, Pulver S R and Marder E 2010 *J. Neurosci.* **30** 4687
[57] Li W C, Merrison-Hort R, Zhang H Y and Borisyuk R 2014 *J. Neurosci.* **34** 6065
[58] Guan L N, Jia B and Gu H G 2019 *Int. J. Bifurcat. Chaos* **29** 1950198